Chemical Physics Letters 627 (2015) 116–120

Contents lists available at ScienceDirect

Chemical Physics Letters

journal homepage: www.elsevier.com/locate/cplett

Prediction of thermal resistances and heat conduction of carbon nanotube aerogels in various permeated gases

Feng Gong [1], Yong Siang Tam [1], Son T. Nguyen, Hai M. Duong *

Department of Mechanical Engineering, National University of Singapore, Singapore, 117576 Singapore

ARTICLE INFO

Article history:
Received 17 December 2014
In final form 20 March 2015
Available online 28 March 2015

ABSTRACT

Heat conduction in single-walled carbon nanotube (SWNT) aerogels is investigated by an off-lattice Monte Carlo method. Thermal boundary resistances (TBRs) between the SWNT and four permeated gases of argon, nitrogen, neon and hydrogen are reported from fitting simulation results with experimental data. It is found that the TBRs between the SWNT and the permeated gases decrease with larger gas molecular masses. Effects of volume fractions and complex morphologies of SWNTs on thermal conductivities of SWNT aerogels are also quantified. The effective thermal conductivities of SWNT aerogels increase with the larger volume fraction, the greater length and the smaller diameter of the SWNTs.

1. Introduction

Aerogels are ultralight and highly porous materials fabricated by subjecting a wet-gel precursor to critical-point drying or freeze-drying to remove liquid without collapsing the network. The aerogels are composed of tenuous networks of clustered nanoparticles, and have unique properties including very high strength-to-weight and surface-area-to-volume ratios. Small diameter carbon nanotubes (CNTs) such as single-walled CNTs (SWNTs) are exciting candidates for electrically conducting aerogels due to their excellent thermal, electrical and mechanical properties [1–4]. Ensembles of such CNTs can form electrically percolating networks at very low volume fractions [5] and elastic gels in concentrated suspensions through van der Waals interaction mediated crosslinking [5–7]. The CNT aerogels can be applied in energy storage systems [8–10], hydrogen storage media [11] and weight-conscious devices such as satellites [5].

The CNT aerogels had the relative high electrical conductivity of 1.0 S/cm [12] and excellent elastic modulus of 60 MPa cm^3 g^{-1} [13]. However, the thermal conductivities of the CNT aerogels were 0.01–0.1 W/mK [5,14], five orders of magnitude lower than that of the intrinsic CNTs (2000–5000 W/m K) [15]. Schiffres et al. [5] studied the thermal conductivity of gas-permeated SWNT aerogels through experiments and modeling using mesoscale and atomistic simulations. The thermal conductivity of their evacuated aerogel was 0.025 W/m K at a temperature of 300 K. The ultralow thermal conductivity of the CNT aerogels may be caused by the high porosity of the CNT aerogels, the thermal boundary resistance (TBR) at air-CNT contact, inter-CNT contact and induced defects of the CNTs during aerogel fabrication processes [16–19].

Environment-dependent studies of thermal transport have been performed on isolated CNT bundles to identify gas-CNT heat transfer coefficients [20,21], yet not in CNT networks. Effects of the CNT accommodation coefficient on gas diffusion through the nanoporous CNT network remain unresolved. Schiffres et al. [5] also reported the nature of gas diffusion in the SWNT aerogel, and the efficiency of energy exchange between gas molecules and the SWNTs using pressure-dependent thermal conductivity measurements and multiscale simulations. Thermal conductivity measurements and analysis of the gas-permeated aerogel (argon Ar, nitrogen N_2, neon Ne, and hydrogen H_2) showed that gas molecules transport energy over length scales hundreds of times larger than the diameters of the pores in the aerogel. This difference was through the low gas SWCNT thermal accommodation coefficient and the open-cell network structure of the SWNT aerogel [5].

Understanding heat transport mechanisms and the TBRs of the CNT aerogels can guide material scientists and application engineers who want to harness the unique thermal and gas-diffusion properties of SWNT aerogels and related nanoporous materials in diverse applications [10,22,23,11]. Due to several limitations of experiment techniques such as measuring the TBR at the interface of the CNTs and surrounding materials, some computational works have been developed to investigate mainly the heat exchange at the interface of the CNT–CNT and the CNT–air [24–26]. But the

* Corresponding author.
E-mail address: mpedhm@nus.edu.sg (H.M. Duong).
[1] These authors contributed equally to this work.

http://dx.doi.org/10.1016/j.cplett.2015.03.035
0009-2614/

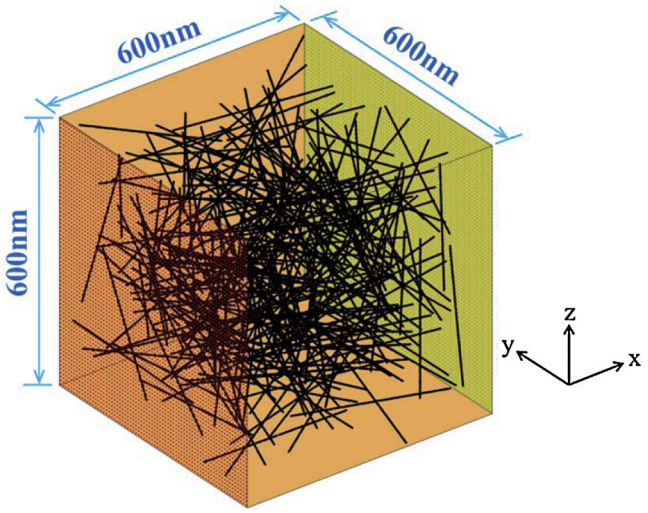

Figure 1. Schematic plot of the computational model: 1049 SWNTs having 2 nm in diameter, 400 nm in length are randomly oriented and distributed in the gas cube with a side length of 600 nm. The plane with red dots represents the heated surface and the plane with green dots is the cooled surface.

mechanisms and limitations of the heat transport of the three dimensional (3D) CNT aerogels have not been studied well through experiments and modeling. Therefore, in this work, we develop a mesoscopic 3D model to investigate the TBR and the heat transport of the SWNT aerogels by using an Off-lattice Monte Carlo method. For the first time, the TBRs between the SWNTs and the permeated gases of Ar, N_2, Ne, and H_2 are estimated by matching the effective thermal conductivity (K_{eff}) of the SWNT aerogels obtained from the simulation results with the experimental data of Schiffres et al. [5]. The effects of concentrations and complex morphologies of the SWNTs on K_{eff} of the SWNT aerogels are quantitatively investigated. The developed model can provide a comprehensive study of the heat transport mechanism of the SWNT aerogels, and also help experimentalists to optimize the thermal properties of the SWNT aerogels through aerogel structure control.

2. Simulation methodology

A 3D model is built based on the SWNT aerogels fabricated by Schiffres et al. [5]. The aerogels have a density of 8 kg/m^3 and 0.61 vol% volume fraction of the SWNTs. Based on the composition of SWNT aerogels, 1049 SWNTs (0.61 vol%) with 2 nm in diameter and 400 nm in length are randomly distributed and oriented in a gas cube with side length of 600 nm, as shown in Figure 1. The gas phase is treated as bulk material without modeling the motion of gas molecules. The gas properties (e.g., thermal conductivity, specific heat and density) can be varied to model the heat conduction of the SWNT aerogels in the different gas environments. In the present work, nitrogen (N_2) is chosen as the study case as N_2 has exactly similar thermophysical properties with air.

In the developed model, heat is quantified by a large quantity of discrete thermal walkers with the same energy. The thermal walkers have a Brownian motion in the gas phase and a random motion in the SWNTs [27,28]. The Brownian motion of thermal walkers in the gas phase is described by random jumps in each space direction [29]. The jump distances take values from a normal distribution with a zero mean and a standard deviation, σ, that is expressed as [30]:

$$\sigma = \sqrt{2D_g \Delta t} \tag{1}$$

where D_g is the thermal diffusivity of the gas and Δt is the duration of a time step in the simulation. The constant heat flux is applied through the computational domain by releasing 40,000 thermal walkers every time step from one side of the model, at $x = 0$. In the meantime, 40,000 cold walkers carrying negative energy are released from the opposite side, representing a cooled surface [28,31].

Due to the thermal boundary resistance present at SWNT–gas interface, phonons from the gas phase may either be reflected to the gas or be transmitted into a SWNT. The average phonon transmission probability from the gas to a SWNT (f_{g-SWNT}) is used to govern the motion of thermal walkers at SWNT–gas interface. Once a thermal walker in the gas phase crosses the interface between the gas and the SWNT, it may either jump into the SWNT with a probability f_{g-SWNT}, or remain in the gas phase with a probability $(1 - f_{g-SWNT})$. According to the acoustic mismatch model (AMM), the probability f_{g-SWNT} is applied to quantify the thermal boundary resistance (TBR) between the gas and the SWNTs, R_{g-SWNT}, as follow [32]:

$$f_{g-SWNT} = \frac{4}{\rho C_P \nu R_{g-SWNT}} \tag{2}$$

where ρ, C_P and ν are the density of the gas, the specific heat of the gas and the speed of sound in the gas, respectively. When the thermal walker jumps into the SWNT, it is assumed to travel at an infinite speed in the SWNT relative to random jump in gas phase due to the ballistic phonon transport property [14] and the ultrahigh thermal conductivity of SWNTs [33]. It means that thermal walkers distribute uniformly in a SWNT once they jump into the SWNT. When the walker in the SWNT travels to the interface between the SWNT and the surrounding gas, it can exit from the SWNT to the gas with a probability f_{SWNT-g}.

In the present model, the TBRs are assumed to be identical at the same interface for thermal walkers entering or exiting from a component (the gas or the SWNTs). According to the second thermodynamic theorem [34], in the thermal equilibrium state, the heat flux entering a SWNT should be equal to that exiting from the SWNT to maintain a constant temperature of the SWNT. All the walkers inside the SWNT can travel to the surrounding gas in one time step due to the infinite speed, while only those walkers around the SWNT surface in the gas may jump into the SWNT because of the random Brownian motion [28]. Therefore, to maintain the same heat flux entering and exiting from the SWNT, the two probabilities, f_{SWNT-g} and f_{g-SWNT}, should satisfy:

$$V_{SWNT} f_{SWNT-g} = C_f \sigma A_{SWNT} f_{g-SWNT} \tag{3}$$

where V_{SWNT} and A_{SWNT} are the volume and surface area of the SWNT, respectively. C_f is the thermal equilibrium factor, which is dependent on the geometry of the SWNTs and the interfacial area between the SWNT and the gas [28].

A model of the pure gas without any SWNT is also built as a reference model to compare and estimate the effective thermal conductivity, K_{eff}, of the SWNT aerogel. Under the same heat flux, q'', and boundary conditions, the temperature distributions along the heat flux (x-direction) in the SWNT aerogel model, T_a, and in the pure gas model, T_g, satisfy:

$$q'' = -K_{eff} \frac{dT_a}{dx} = -K_g \frac{dT_g}{dx} \tag{4}$$

wherein K_g is the thermal conductivity of the pure gas. The model is divided into a $300 \times 300 \times 300$ grid mesh. The temperature at the specific position of the computational box is obtained by counting the number of hot walkers with subtracting the number of cold walkers in each grid cell [35]. Then the effective thermal conductivity of the SWNT aerogels can be calculated as:

$$K_{eff} = K_g \left(\frac{dT_g/dx}{dT_a/dx} \right) \tag{5}$$

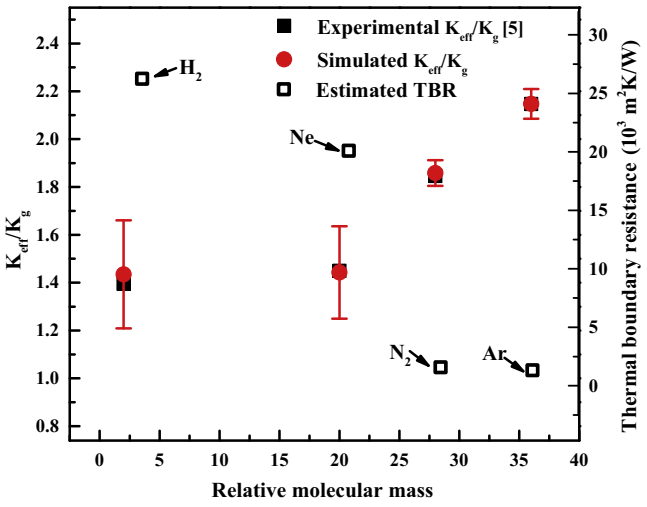

Figure 2. The match between simulated and measured effective thermal conductivity of the SWNT aerogels, and the thermal boundary resistances (TBRs) between the SWNTs and H_2, Ne, N_2 and Ar gases under the atmospheric pressure and the room temperature. The error bars are the standard deviations of 3 simulation results using different spatial distribution of SWNTs. The experimental results are taken from Ref. [5].

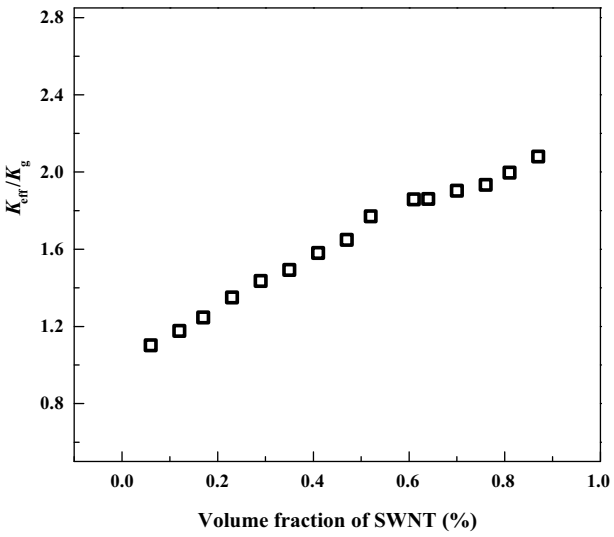

Figure 3. Effects of the SWNT volume fractions on the K_{eff} of the SWNT aerogels. The 2 nm-diameter and 400-nm length of the SWNT are kept constant. Nitrogen (N_2) is chosen as a study case here.

The assumptions made in the developed model are: (i) collisions between thermal walkers are ignored; (ii) the properties of the gas and the SWNTs (e.g., density, thermal conductivity, specific heat capacity) do not change with the temperature over the modeled range; (iii) the TBRs at SWNT contacts are not considered due to the pi-pi interactions between SWNTs [36]; (iv) the model is a representative volume element of the practical aerogel, so the convection effect is not considered [37]; (v) periodic boundary conditions are applied in *y*- and *z*-directions, while walkers are bounced back when jumping outside the computational box in the *x*-direction; (vi) the model has the same initial temperature; and (vii) effects of a binder connecting the SWNTs are ignored.

3. Results and discussions

3.1. Estimated thermal boundary resistances (TBRs) between the SWNTs and the different gases in the 3D SWNT aerogels

By matching the effective thermal conductivity of the SWNT aerogels obtained from the simulations with those from experimental measurement in the different gas environments (Ar, N_2, Ne and H_2) under the atmospheric pressure and the room temperature [5], the TBRs between the SWNTs and the above gases are estimated, as presented in Figure 2. The TBRs between the SWNTs and Ar, N_2, Ne and H_2 are 1.32×10^{-3}, 1.57×10^{-3}, 20.1×10^{-3} and 26.5×10^{-3} m^2 K/W, respectively. The TBRs between the SWNTs and the gases decrease with increasing the gas molecular mass under the atmospheric pressure and the room temperature. This finding is consistent with the reported findings in molecular dynamics (MD) approaches [24,38]. Since the heavier gas atoms have lower velocities, they may have longer interaction time with the SWNTs. This may induce a higher energy accommodation coefficient and thus a lower TBR between the gas and the SWNT [24].

It is noted that Schiffres et al. [5] also estimated the energy accommodation coefficient of various gases by MD simulations. The TBR between gas and SWNTs (R_{g-SWNT}) can be calculated from the energy accommodation coefficient by [24]:

$$R_{g-SWNT} = \frac{2-\alpha}{4k_B N\alpha} \quad (6)$$

where α, k_B and N are the energy accommodation coefficient, the Boltzmann constant and the gas collision rate on the SWNT surface per unit area, respectively. In Schiffres et al. work [5], only two concentric SWNTs with 40 nm length were used. This length is much shorter than those of SWNTs in the experimental samples (~300–1000 nm) [5]. Thus, the effect of quantity and length of SWNTs on the heat exchange between gas and SWNTs may be misinterpreted and underestimated. To break the above limitation in Schiffres et al. MD approach, in this work, the developed model is built with thousands of SWNTs to replicate the real SWNT aerogel samples. The length and diameter of the SWNTs are also consistent with those in the experimental sample. Moreover, the off-lattice Monte Carlo algorithm applied in this work is much faster than MD simulations [27,30].

Since the experimental data of the TBRs between the pure gases and the SWNTs are still very limited, the measured TBR between the SWNT and air is used to compare our estimated TBR between the SWNT and N_2. Hsu et al. [20] reported the TBR between air and the SWNT to be $\sim 0.7 \times 10^{-3}$ m^2 K/W measured by a two-laser technique. The TBR between N_2 and the SWNT is estimated to be $\sim 1.5 \times 10^{-3}$ m^2 K/W in the present work. The slight discrepancy between our simulated TBR and the measured TBR may be caused by the molecular mass difference of N_2 and air. Under the atmospheric pressure and the room temperature, the air consisting of 78 vol% N_2 and 21 vol% O_2 is heavier than the pure N_2. It has longer interaction time with the SWNT, leading to a slight lower TBR between air and the SWNT. It is noted that the TBRs between the SWNT and gases are higher than those at the SWNT–liquid and the SWNT–solid interfaces ($\sim 10^{-5}$–10^{-9} m^2 K/W) [39–42]. The higher TBRs at SWNT–gas interfaces may be ascribed to the greater acoustic mismatch between the SWNTs and gases, as well as the stronger phonon scattering at SWNT–gas interfaces.

3.2. Effects of the SWNT volume fractions on the effective thermal conductivity (K_{eff}) of the SWNT aerogels

The volume fractions of the SWNTs in the SWNT aerogels are quantified by varying the number of the SWNTs randomly distributed in the model. The volume fraction of the SWNTs varies from 0.06 vol% to 0.87 vol% (100–1500 SWNTs). The effects of the SWNT volume fractions on the K_{eff} of the SWNT aerogels are presented in Figure 3. The K_{eff} of the SWNT aerogels increases with the

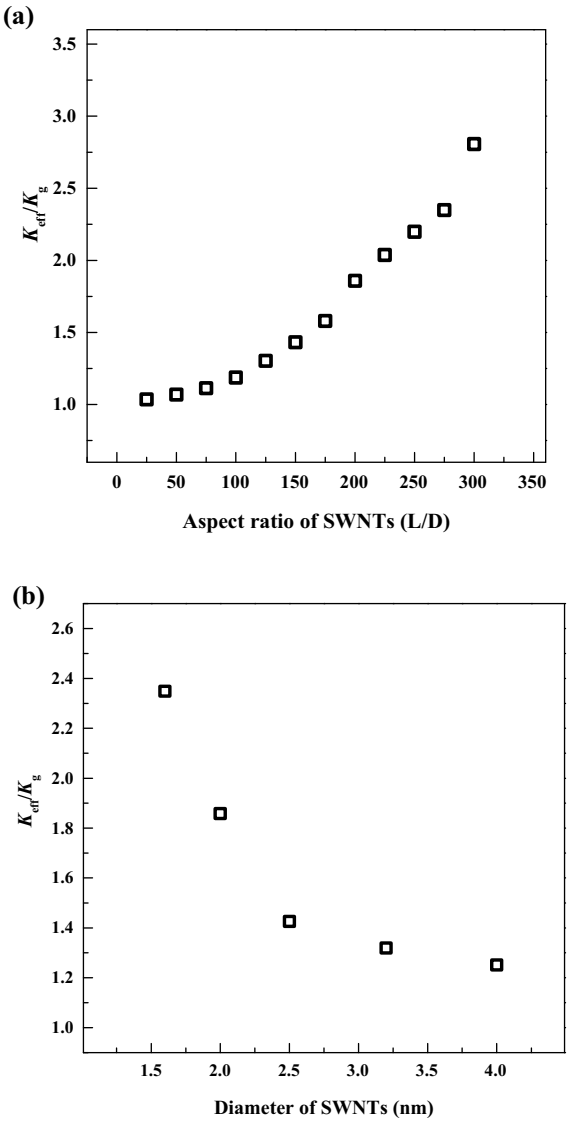

Figure 4. Effects of (a) aspect ratios of 25–300 (length = 50–600 nm, diameter = 2 nm) and (b) diameter of 1.6–4 nm (length = 400 nm) of the SWNTs on the K_{eff} of the SWNT aerogels. The volume fraction of the SWNTs is keep constant to be 0.61 vol%. Nitrogen gas (N_2) is used in the simulations of this figure.

increase of the SWNT volume fraction. More SWNTs not only reduce the porosity of the aerogel, but also provide more phonon transport paths. Owing to the ultrahigh thermal conductivity of the SWNTs, they can act as the effective thermal transport channels, which allow the thermal walker to travel faster in the SWNT aerogels. Hence the higher thermal conductivity of the SWNT aerogels can be achieved and this trend is also consistent with the experiment findings [37].

3.3. Effects of the SWNT morphologies on the effective thermal conductivity (K_{eff}) of the SWNT aerogels

3.3.1. Effects of the SWNT aspect ratios

Though the SWNTs can exhibit a high aspect ratio (length/diameter) of up to 1000 [43], the effects of the common aspect ratios of 25–300 of the SWNTs on the K_{eff} of the SWNT aerogels are chosen to be investigated in this work. The SWNT length varies from 50 to 600 nm while the diameter of the SWNTs is kept constant to be 2 nm (aspect ratio from 25 to 300). Figure 4(a) presents the K_{eff} of the SWNT aerogels using the SWNTs with various aspect ratios. The K_{eff} of the SWNT aerogels increases when the SWNT aspect ratio rises. With the same diameter, the SWNTs with a higher aspect ratio have a longer length. Due to the ballistic phonon transport in the SWNTs and the diffusive thermal transport in gases, SWNTs are much more effective heat transfer channels than gases in SWNT aerogels [14,33]. Longer SWNTs more effectively transport heat through the aerogels than the short SWNTs [44]. This thereby leads to the higher thermal conductivity of the SWNT aerogels. This quantitative finding is in consistency with the experimental findings in CNT based nanofluid and polymer composite [44,45]. On the other hand, during the practical fabrication of the SWNT aerogels, the longer SWNTs may have a lower percolation threshold than the short ones. The lower percolation threshold means that the longer SWNTs with a lower volume fraction can provide the aerogels with the enhanced electrical and thermal conductivity comparable to those achieved by the short SWNTs with a much higher volume fraction [46].

3.3.2. Effects of the SWNT diameter

The SWNT diameter varies from 1.6 to 4 nm while the SWNT length is kept constant to be 400 nm. As shown in Figure 4(b), the K_{eff} of the SWNT aerogels decreases as the diameter of SWNTs increases. This may be explained physically that (i) with the same volume fraction and the same length, the SWNTs with the smaller diameters have larger total surface area than those with the larger diameters. The larger surface area of the SWNTs can significantly enhance the heat exchange between SWNTs and the gases, resulting in a higher K_{eff} of the SWNT aerogels [47,48]. (ii) The larger diameters of SWNTs make heat more transport in the radial direction, reducing the heat conduction in the SWNT axial direction and the heat flux direction, and hence leading to a lower K_{eff} of the SWNT aerogels. This finding is also consistent with our previous works [31,49,50]. Due to the ballistic thermal transport in SWNTs and the diffusive heat transport in gases, SWNTs dominate the transfer of heat in SWNT aerogels. We speculate that effects of SWNT morphologies (e.g., length and diameter) on the thermal transport properties of SWNT aerogels in different gases will be qualitatively similar.

4. Conclusions

A 3D mesoscopic model is successfully developed to investigate the TBRs and the heat transport in the SWNT aerogels. The TBRs between the SWNTs and four surrounding gases are estimated and they decreases with the larger gas molecular mass. Effects of the volume fractions and the morphologies of the SWNTs on the thermal properties of the SWNT aerogels are also quantitatively investigated. The simulation results show that the higher SWNT volume fraction, the longer length and the smaller diameter of the SWNTs could result in a higher K_{eff} of the SWNT aerogels. The developed model can be also applied to study the heat transport phenomena and limitations in other diverse aerogels and highly porous materials such as graphene aerogels, carbon aerogels and silicon aerogels.

Acknowledgements

The authors would like to thank SERC 2011 PSF Funding R-265-000-424-305 and Temasek Laboratories @ NUS Funding R-394-001-077-232 for the financial support.

Appendix A. Supplementary data

Supplementary material related to this article can be found, in the online version, at doi:10.1016/j.cplett.2015.03.035.

References

[1] M.F.L. De Volder, S.H. Tawfick, R.H. Baughman, A.J. Hart, Science 339 (2013) 535.
[2] J.C. Blancon, M. Paillet, H.N. Tran, X.T. Than, S.A. Guebrou, A. Ayari, A. San Miguel, N.M. Phan, A.A. Zahab, J.L. Sauvajol, N. Del Fatti, F. Vallee, Nat. Commun. (2013) 4.
[3] Q. Zhang, J.-Q. Huang, W.-Z. Qian, Y.-Y. Zhang, F. Wei, Small 9 (2013) 1237.
[4] J.N. Coleman, U. Khan, W.J. Blau, Y.K. Gun'ko, Carbon 44 (2006) 1624.
[5] S.N. Schiffres, K.H. Kim, L. Hu, A.J.H. McGaughey, M.F. Islam, J.A. Malen, Adv. Funct. Mater. 22 (2012) 5251.
[6] K.H. Kim, M. Vural, M.F. Islam, Adv. Mater. 23 (2011) 2865.
[7] M.B. Bryning, D.E. Milkie, M.F. Islam, L.A. Hough, J.M. Kikkawa, A.G. Yodh, Adv. Mater. 19 (2007) 661.
[8] V. Presser, M. Heon, Y. Gogotsi, Adv. Funct. Mater. 21 (2011) 810.
[9] J. Biener, M. Stadermann, M. Suss, M.A. Worsley, M.M. Biener, K.A. Rose, T.F. Baumann, Energy Environ. Sci. 4 (2011) 656.
[10] Y. Zhai, Y. Dou, D. Zhao, P.F. Fulvio, R.T. Mayes, S. Dai, Adv. Mater. 23 (2011) 4828.
[11] B. Assfour, S. Leoni, G. Seifert, I.A. Baburin, Adv. Mater. 23 (2011) 1237.
[12] J.H. Zou, J.H. Liu, A.S. Karakoti, A. Kumar, D. Joung, Q.A. Li, S.I. Khondaker, S. Seal, L. Zhai, ACS Nano 4 (2010) 7293.
[13] K.H. Kim, Y. Oh, M.F. Islam, Nat. Nanotechnol. 7 (2012) 562.
[14] K.J. Zhang, A. Yadav, K.H. Kim, Y. Oh, M.F. Islam, C. Uher, K.P. Pipe, Adv. Mater. 25 (2013) 2926.
[15] Z.D. Han, A. Fina, Prog. Polym. Sci. 36 (2011) 914.
[16] Z. Fan, D.Z.Y. Tng, C.X.T. Lim, P. Liu, S.T. Nguyen, P. Xiao, A. Marconnet, C.Y.H. Lim, H.M. Duong, Colloids Surf. A: Physicochem. Eng. Aspects 445 (2014) 48.
[17] Z. Fan, D.Z.Y. Tng, S.T. Nguyen, J.D. Feng, C.F. Lin, P.F. Xiao, L. Lu, H.M. Duong, Chem. Phys. Lett. 561 (2013) 92.
[18] S.T. Nguyen, H.T. Nguyen, A. Rinaldi, N.P.V. Nguyen, Z. Fan, H.M. Duong, Colloids Surf. A: Physicochem. Eng. Aspects 414 (2012) 352.
[19] K.H. Kim, Y. Oh, M.F. Islam, Adv. Funct. Mater. 23 (2013) 377.
[20] I.-K. Hsu, M.T. Pettes, M. Aykol, C.-C. Chang, W.-H. Hung, J. Theiss, L. Shi, S.B. Cronin, J. Appl. Phys. 110 (2011).
[21] I.K. Hsu, M.T. Pettes, M. Aykol, S. Li, S.B. Cronin, J. Appl. Phys. 108 (2010), 084307-084307-084304.
[22] M. Schmidt, F. Schwertfeger, J. Non-Cryst. Solids 225 (1998) 364.
[23] R.R. Mitchell, B.M. Gallant, C.V. Thompson, Y. Shao-Horn, Energy Environ. Sci. 4 (2011) 2952.
[24] L. Hu, A.J.H. McGaughey, J. Phys. Chem. C 117 (2013) 18804.
[25] M. Hu, S. Shenogin, P. Keblinski, N. Raravikar, Appl. Phys. Lett. 90 (2007).
[26] H.-D. Wang, J.-H. Liu, X. Zhang, T.-Y. Li, R.-F. Zhang, F. Wei, J. Nanomater. 2013 (2013) 7.
[27] H.M. Duong, D.V. Papavassiliou, K.J. Mullen, S. Maruyama, Nanotechnology 19 (2008) 065702.
[28] F. Gong, D.V. Papavassiliou, H.M. Duong, Numer. Heat Transf. A: Appl. 65 (2014) 1023.
[29] H.M. Duong, N. Yamamoto, D.V. Papavassiliou, S. Maruyama, B.L. Wardle, Nanotechnology 20 (2009) 155702.
[30] H.M. Duong, D.V. Papavassiliou, L.L. Lee, K.J. Mullen, Appl. Phys. Lett. 87 (2005) 013101.
[31] F. Gong, K. Bui, D.V. Papavassiliou, H.M. Duong, Carbon 78 (2014) 305.
[32] E.T. Swartz, R.O. Pohl, Rev. Modern Phys. 61 (1989) 605.
[33] A.A. Balandin, Nat. Mater. 10 (2011) 569.
[34] K. Bui, D.V. Papavassiliou, Numer. Heat Transf. A: Appl. 63 (2013) 590.
[35] K. Bui, B.P. Grady, D.V. Papavassiliou, Chem. Phys. Lett. 508 (2011) 248.
[36] Z. Fan, F. Gong, S.T. Nguyen, H.M. Duong, Carbon 81 (2015) 396.
[37] Z. Fan, A. Marconnet, S.T. Nguyen, C.Y.H. Lim, H.M. Duong, Int. J. Heat Mass Transf. 76 (2014) 122.
[38] K.J. Daun, T.A. Sipkens, J.T. Titantah, M. Karttunen, Appl. Phys. B – Lasers Opt. 112 (2013) 409.
[39] S.T. Huxtable, D.G. Cahill, S. Shenogin, L.P. Xue, R. Ozisik, P. Barone, M. Usrey, M.S. Strano, G. Siddons, M. Shim, P. Keblinski, Nat. Mater. 2 (2003) 731.
[40] H. Zhong, J.R. Lukes, Phys. Rev. B 74 (2006) 125403.
[41] C.F. Carlborg, J. Shiomi, S. Maruyama, Phys. Rev. B 78 (2008).
[42] S. Kumar, M.A. Alam, J.Y. Murthy, Appl. Phys. Lett. 90 (2007).
[43] S. Shenogin, A. Bodapati, L. Xue, R. Ozisik, P. Keblinski, Appl. Phys. Lett. 85 (2004) 2229.
[44] A.S. Cherkasova, J.W. Shan, J. Heat Transf. – Trans. ASME 132 (2010) 082402.
[45] R.S. Kapadia, B.M. Louie, P.R. Bandaru, J. Heat Transf. – Trans. ASME 136 (2014).
[46] K. Shehzad, M.N. Ahmad, T. Hussain, M. Mumtaz, A.T. Shah, A. Mujahid, C. Wang, J. Ellingsen, Z.-M. Dang, J. Appl. Phys. 116 (2014).
[47] W.T. Jiang, G.L. Ding, H. Peng, Int. J. Thermal Sci. 48 (2009) 1108.
[48] X.-Q. Wang, A.S. Mujumdar, Int. J. Thermal Sci. 46 (2007) 1.
[49] F. Gong, Z. Hongyan, D.V. Papavassiliou, K. Bui, C. Lim, H.M. Duong, Nanotechnology 25 (2014) 205101.
[50] H.M. Duong, N. Yamamoto, K. Bui, D.V. Papavassiliou, S. Maruyama, B.L. Wardle, J. Phys. Chem. C 114 (2010) 8851.